Applied Physics Letters

RESEARCH ARTICLE | MAY 24 2021

Anomalous layer-dependent electronic and piezoelectric properties of 2D $GaInS_3$ nanosheets

Weizhen Chen; Huabing Yin; Shujuan Jiang; Siyuan Liu; Chang Liu; Bing Wang; Guang-Ping Zheng

Check for updates

Appl. Phys. Lett. 118, 213103 (2021)
https://doi.org/10.1063/5.0050854

View Online
Export Citation

Articles You May Be Interested In

Piezoelectric biaxial strain effects on the optical and photoluminescence spectra of 2D III–VI compound α -In_2Se_3 nanosheets

Appl. Phys. Lett. (March 2020)

Switchable valley polarization and quantum anomalous Hall state in the $VN_2X_2Y_2$ nanosheets (X = group-III and Y = group-VI elements)

Appl. Phys. Lett. (November 2021)

Ab initio simulation studies on the room-temperature ferroelectricity in two-dimensional β -phase GeS

Appl. Phys. Lett. (May 2019)

31 December 2024 04:21:12

AIP Publishing

Applied Physics Letters

Special Topics Open for Submissions

Learn More

AIP Publishing

Applied Physics Letters ARTICLE scitation.org/journal/apl

Anomalous layer-dependent electronic and piezoelectric properties of 2D $GaInS_3$ nanosheets

Cite as: Appl. Phys. Lett. **118**, 213103 (2021); doi: 10.1063/5.0050854
Submitted: 19 March 2021 · Accepted: 9 May 2021 ·
Published Online: 24 May 2021

View Online Export Citation CrossMark

Weizhen Chen,[1] Huabing Yin,[1,a)] Shujuan Jiang,[1] Siyuan Liu,[1] Chang Liu,[1] Bing Wang,[1,a)] and Guang-Ping Zheng[2,a)]

AFFILIATIONS

[1]Institute for Computational Materials Science, School of Physics and Electronics, International Joint Research Laboratory of New Energy Materials and Devices of Henan Province, Henan University, Kaifeng 475004, China
[2]Department of Mechanical Engineering, The Hong Kong Polytechnic University, Hung Hom, Kowloon, Hong Kong 999077, China

[a)]Authors to whom correspondence should be addressed: yhb@henu.edu.cn; wb@henu.edu.cn; and mmzheng@polyu.edu.hk

ABSTRACT

Two-dimensional (2D) $GaInS_3$ nanosheets are found to exhibit thermal and structural stabilities, good oxidation resistance, and tunable and layer-dependent electronic properties from first-principles calculations. Remarkably, the nanosheets with arbitrary thickness possess robust in-plane piezoelectricity without the odd-even effect commonly observed in other 2D piezoelectric materials, which is attributed to the retention of noncentrosymmetry resulting from their homogeneous and direct stacking patterns. The piezoelectric stress coefficient e_{11}^{3D} of the nanosheets is about 0.23 C/m^2, almost independent of the numbers of atomic layers of 2D $GaInS_3$. The stability in piezoelectricity and the high carrier mobility of 2D $GaInS_3$ nanosheets could endow them with promising application prospects in nanoelectronic and nanoelectromechanical devices.

Published under an exclusive license by AIP Publishing. https://doi.org/10.1063/5.0050854

31 December 2024 04:21:12

Because of the increasing demands for miniaturization and multifunctionality in piezoelectric devices, two-dimensional (2D) piezoelectric materials have stimulated much research interest in the past decade.[1–4] Theoretical predictions on various 2D materials, such as metal oxides,[5,6] transition metal dichalcogenides,[7] group-II/III/IV monochalcogenides,[6,8,9] group-III-V compounds,[10] and group-V binary compounds,[11] have revealed that some of them possess ultrahigh piezoelectric coefficients. Meanwhile, from experimental studies, 2D monolayer *2H*-MoS_2 and *h*-BN are reported to exhibit piezoelectricity with coefficients comparable to those of conventional bulk materials.[3,4,12]

For device applications, 2D materials are generally utilized in the form of multilayered nanosheets. Thus, a layer-dependent piezoelectric behavior of 2D materials has to be considered in the devices. Unfortunately, the piezoelectricity of most reported 2D materials, such as 2*H*-MoS_2, exists only in monolayer or multilayer materials and decreases gradually with increasing layer number.[3] More seriously, since the alternating layers of those nanosheets are stacked alternatively with an opposite orientation, multilayered nanosheets with an even number of layers are centrosymmetric and can lose their piezoelectric response,[1,3] while only the odd-layer nanosheets with a broken inversion symmetry can exhibit piezoelectricity. Such odd-even effect of piezoelectricity in 2D materials increases the difficulty in materials preparation and limits their practical applications. Although the piezoelectricity in both monolayer and multilayer α-In_2Se_3 nanosheets with a noncentrosymmetric hexagonal stacking pattern was observed recently,[13] the 2D piezoelectric materials without any odd-even effect are still quite limited.

In this Letter, based on first-principles calculations, we report an unexplored 2D $GaInS_3$ material that can be exfoliated from its bulk crystal, which is first synthesized in 1987.[14] $GaInS_3$ is a typical semiconductor with a wide bandgap varying from 3.04 eV for the monolayer to 2.66 eV of the bulk. It is revealed that this material possesses anomalous layer-dependent piezoelectricity compared with previously reported 2D piezoelectric materials. Remarkably, it is found that both odd- and even-layer $GaInS_3$ are piezoelectric, attributing to the retention of noncentrosymmetry because of their homogeneous and direct stacking patterns. Moreover, the theoretical calculations also show that 2D $GaInS_3$ have good structural stability, excellent oxidation resistance, and high carrier mobility. Such robust piezoelectricity

Published under an exclusive license by AIP Publishing

accompanying with tunable electronic properties ensure that 2D $GaInS_3$ nanosheets could be widely utilized in nanoelectronic and nanoelectromechanical devices.

All first-principles calculations were carried out within the framework of density functional theory (DFT) by using the Vienna *Ab initio* Simulation Package (VASP) code.[15–17] Generalized gradient approximation (GGA) within the Perdew–Burke–Ernzerhof (PBE) method was employed to describe exchange–correlation potential.[18] A plane wave basis set within a kinetic cutoff energy of 500 eV was used. The interactions between electrons and nuclei were described within the projector-augmented wave (PAW) method.[16,19] The Brillouin zone was sampled using mesh sizes of $8 \times 12 \times 1$ for 2D systems and $7 \times 7 \times 4$ for 3D bulk in the Monkhorst–Pack scheme.[20] Electronic properties were also examined by the Heyd–Scuseria–Ernzerhof (HSE) hybrid functional.[21] To eliminate the interactions between neighboring images of the supercells, a vacuum layer with a thickness of 20 Å perpendicular to the monolayer was added. The convergence criterions for the total energy and force were set to be 10^{-6} eV and 10^{-3} eV/Å, respectively. The interlayer and intralayer van der Waals corrections were treated by the Grimme's DFT-D3 scheme.[22] The phonon spectrum was calculated using the density functional perturbation theory (DFPT) as implemented in the PHONOPY package within a $3 \times 3 \times 1$ supercell.[23] *Ab initio* molecular dynamics (AIMD) simulations are performed on a $4 \times 4 \times 1$ supercell by using a canonical ensemble (NVT).[24]

As illustrated in the supplementary material, Fig. S1(a), bulk $GaInS_3$, characterized by an orthorhombic crystal structure, is a natural pseudo-2D crystal with the $Cmc2_1$ (No. 36) space group. The optimized lattice parameters of bulk $GaInS_3$ are $a = b = 9.81$ Å, $c = 6.19$ Å, and $\gamma = 157.75°$, which are in good agreement with the experimental values ($a = b = 9.93$ Å, $c = 6.22$ Å, and $\gamma = 157.92°$).[14] Bulk $GaInS_3$ is an indirect semiconductor with a bandgap of 2.66 eV at the HSE level [see the supplementary material, Fig. S1(c)], which is in a moderate bandgap region as compared with those of previously reported wide-bandgap InTeI (2.32 eV) and GaTeCl (2.96 eV) bulk crystals.[25,26] Similar to other 2D materials, such as graphene, phosphorene, and MoS_2, the natural layered structure of bulk $GaInS_3$ is very beneficial to the formation of 2D monolayer and multilayers.

As shown in Fig. 1(a), the $GaInS_3$ monolayer is stabilized into an orthorhombic structure (space group $Pmn2_1$, No. 31). The calculated lattice constants of $GaInS_3$ monolayer are $a = 6.21$ Å and $b = 3.78$ Å, as listed in the supplementary material, Table S1. The atomic layer is composed of alternative 4- and 6-membered rings containing both Ga–S and In–S bonds. More specifically, each Ga atom forms four covalent bonds with adjacent S atoms, and the bond lengths of Ga–S are 2.25–2.34 Å, while each In atom forms six covalent bonds with S atoms and the In–S bond length is 2.56–2.70 Å. The complicated bonding scheme endows $GaInS_3$ monolayer with a relatively larger thickness (about 7.19 Å) as compared with those of other 2D monolayer materials. Since the successful preparation of monolayer and multilayer $GaInS_3$ is of vital importance to the subsequent studies on their properties, the cleavage process is thus investigated and a cleavage energy of around 0.28 J/m^2 can be obtained for $GaInS_3$ monolayer, notably smaller than that of black phosphorene (0.40 J/m^2), as shown in Fig. 1(b). Such small cleavage energy suggests that the $GaInS_3$ monolayer may be synthesized by mechanical or liquid exfoliation from its 3D bulk crystal.

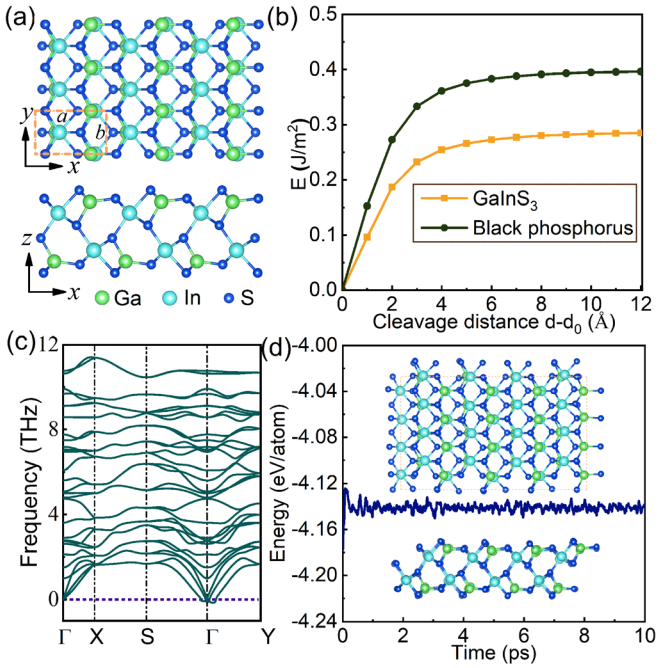

FIG. 1. (a) Top and side views of the optimized structure of monolayer $GaInS_3$. The primitive cell is outlined by dashed lines. (b) Cleavage energy E as a function of separation distance between two layers. (c) The phonon dispersion spectrum of monolayer $GaInS_3$. (d) The evolution of total energy during the AIMD simulations at 300 K. The inset shows the snapshot of an atomic structure at 10 ps.

We then examine the dynamical and thermal stability of $GaInS_3$ monolayer by the phonon dispersion spectrum and AIMD simulation. As plotted in Fig. 1(c), no appreciable negative frequency is found in the phonon band structures, indicating that the $GaInS_3$ monolayer is dynamically stable. Figure 1(d) shows that $GaInS_3$ monolayer maintains its original geometry perfectly without any structural deformation and the total-energy fluctuation is small during the AIMD simulation at 300 K for 10 ps, indicating that $GaInS_3$ monolayer is also thermally stable at room temperature. Furthermore, we perform the AIMD simulation to explore the interaction between the $GaInS_3$ monolayer and gaseous phase O_2 at room temperature. The phenomena of O_2 dissociation have not been found on the $GaInS_3$ surface [see the supplementary material, Fig. S2], which indicates the good oxidation resistance of 2D $GaInS_3$.

As shown in Fig. 2(a), $GaInS_3$ monolayer possesses an indirect bandgap of 2.06 eV at the PBE level and 3.04 eV at the HSE level. The conduction band minimum (CBM) is located at the Γ point, whereas the valence band maximum (VBM) is located along the Γ-X line. Moreover, the VBM is almost dominated by the S atoms, while the CBM is mainly contributed by the In and S atoms [see Figs. 2(b) and 2(c)]. Such a large bandgap is close to those of some traditional wide-bandgap semiconductors, such as SiC (3.2 eV) and ZnO (3.35 eV),[27,28] which endows $GaInS_3$ monolayer with active response to blue and ultra-violet light and promotes its application in light emitting diodes and photodetectors.[29] Notably, the band edge of VBM is extremely flat along the Γ–X line, suggesting that $GaInS_3$ monolayer possesses a quasi-direct bandgap of 3.07 eV at the Γ point. The small energy

31 December 2024 04:21:12

Published under an exclusive license by AIP Publishing

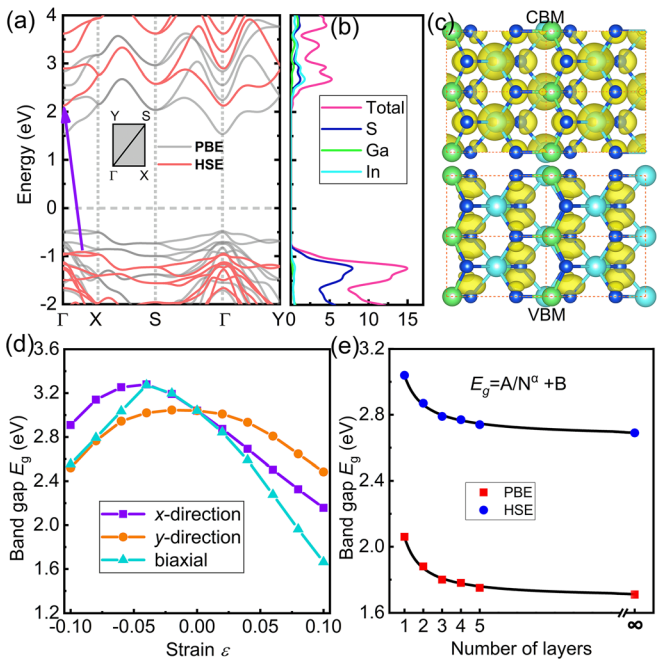

FIG. 2. (a) Band structures and (b) DOS of monolayer $GaInS_3$. The Fermi level is set at zero. (c) Electron density distribution at conduction band minimum (CBM) and VBM. (d) Evolution of the HSE bandgap of monolayer $GaInS_3$ under the applied strains. (e) Evolution of bandgap calculated by PBE and HSE (solid symbols) as a function of the layer number of $GaInS_3$ nanosheets, which is fitted by a power-law curve (solid lines).

difference of 0.03 eV between indirect and quasi-direct bandgaps indicates that the indirect-to-direct bandgap transition may be achieved in the $GaInS_3$ monolayer under very small external perturbations such as the in-plane strain.

The external applied strain has been demonstrated as an effective method to modulate the physical properties of 2D materials because of their excellent mechanical flexibility.[2,30–33] Herein, the changes in the band structure and bandgap of $GaInS_3$ monolayer under various applied uniaxial and biaxial stains are studied. The HSE bandgaps of $GaInS_3$ monolayer as a function of in-plane stain are shown in Fig. 2(d), and the corresponding band structures are plotted in the supplementary material, Figs. S3–S5. Clearly, the bandgaps of $GaInS_3$ monolayer can be tuned in a large range of 1.66–3.28 eV under the strain within ±10%. Actually, the obvious strain sensitivity of the bandgap is induced by the competition between the energies of several band edge states around Γ point, i.e., under the applied uniaxial and biaxial strains, the location of VBM varies from Γ-X line to Γ-Y line and Γ point, while the location of CBM switches between Γ and S points. Moreover, an indirect-to-direct bandgap transition can be achieved under a small compressive strain of 4% along the *x*-direction, and the direct bandgap can be retained with increasing compressive strains [see the supplementary material, Fig. S3]. As we all know, the direct bandgap is favorable for the low-energy optical excitation. Thus, the optical properties of $GaInS_3$ monolayer would be effectively adjusted by strains. Our study suggests that the $GaInS_3$ monolayer is promising for applications in optoelectronic devices.

The geometric parameters and electronic band structures of $GaInS_3$ nanosheets with different numbers of layers ($N = 2$–5) are investigated, which are generated through directly extracting from their bulk crystal. From monolayer (1L) to multilayer (2L–5L) $GaInS_3$, the location of VBM varies from the Γ-X line to Γ-Y line, whereas the location of CBM remains unchanged (see the supplementary material, Fig. S6). Meanwhile, one can find that the addition of more layers induces the obvious band splitting over the entire Brillouin zone, which leads to a slight decrease in the gap. The bandgaps of $GaInS_3$ nanosheets are also plotted in Fig. 2(e), showing that the HSE bandgap changes from 3.04 eV (monolayer) to 2.66 eV (bulk), in consistent with those PBE results. The thickness dependence bandgaps E_g could be described by an exponential decay function $E_g = A/N^{\alpha} + B$, where A, B, and α are the fitted parameters as listed in the supplementary material, Table S2. It is worth noting that the relationship between the HSE-calculated bandgap and N follows the $1/N^{0.94}$ power law for $GaInS_3$, similar to those previously reported in phosphorene and Bi_2Te_2X (X = S, Se) monolayer,[34,35] while the ordinary quantum confinement predicts a much faster decay relationship of $1/N^2$.

Remarkably, the C_{2v} noncentrosymmetry is always maintained in the $GaInS_3$ nanosheets. The piezoelectric stress tensor e_{ijk} and strain tensor d_{ijk} are defined as[36]

$$e_{ijk} = \frac{\partial P_i}{\partial \varepsilon_{jk}}, d_{ijk} = \frac{\partial P_i}{\partial \sigma_{jk}}, \tag{1}$$

where P_i, ε_{jk}, and σ_{jk} are the polarization, strain, and stress tensors, respectively, and

$$e_{ijk} = \frac{\partial P_i}{\partial \varepsilon_{ijk}} = \frac{\partial P_i}{\partial \sigma_{mn}} \cdot \frac{\partial \sigma_{mn}}{\partial \varepsilon_{jk}} = d_{imn} C_{mnjk}, \tag{2}$$

where C_{mnjk} represent elastic stiffness constants. In the Voigt notation,[36] for 2D $GaInS_3$ nanosheets with the C_{2v} point group, the independent coefficients e_{11}, e_{12}, d_{11}, and d_{12} are as follows:

$$d_{11} = \frac{e_{11}C_{22} - e_{12}C_{12}}{C_{11}C_{22} - C_{12}^2}, d_{12} = \frac{e_{12}C_{11} - e_{11}C_{12}}{C_{11}C_{22} - C_{12}^2}. \tag{3}$$

Based on Berry's phase approximation,[37,38] e_{11} and e_{12} are determined from the polarization changes (ΔP) vs uniaxial strains (ε_{11} and ε_{22}) ranging from −0.01 to 0.01 with a step of 0.005. As shown in Figs. 3(a) and 3(b), the slopes of the fitted lines represent the 2D piezoelectric coefficients e_{11}^{2D} and e_{12}^{2D}, and the relaxed-ion condition means that the corresponding coefficients include both the ionic and electronic contributions. To compare with the values for 3D bulk of the same stoichiometry, the 2D piezoelectric coefficients must be renormalized by the effective thickness h of the corresponding nanosheets, i.e., $e_{11}^{3D} = e_{11}^{2D}/h$ and $e_{12}^{3D} = e_{12}^{2D}/h$. The calculated e_{11}^{2D} and e_{12}^{2D} of $GaInS_3$ monolayer are 2.23×10^{-10} and 0.38×10^{-10} C/m, respectively, exhibiting obvious anisotropy. With the increase in layer number N, e_{11}^{2D} and e_{12}^{2D} increase linearly and reach 11.20×10^{-10} and 1.98×10^{-10} C/m for five-layer $GaInS_3$, respectively (see the supplementary material, Table S3). For comparison, the e_{11}^{2D} and e_{11}^{3D} of $GaInS_3$, *h*-BN, and 2*H*-MoS_2 nanosheets and bulk crystals, respectively, are plotted in Figs. 3(c) and 3(d).

Obviously, since the *h*-BN and 2*H*-MoS_2 nanosheets are in an inversely stacking structure of the unit cell along the polarization direction, those with even layers have an inversion symmetry and are

31 December 2024 04:21:12

Published under an exclusive license by AIP Publishing

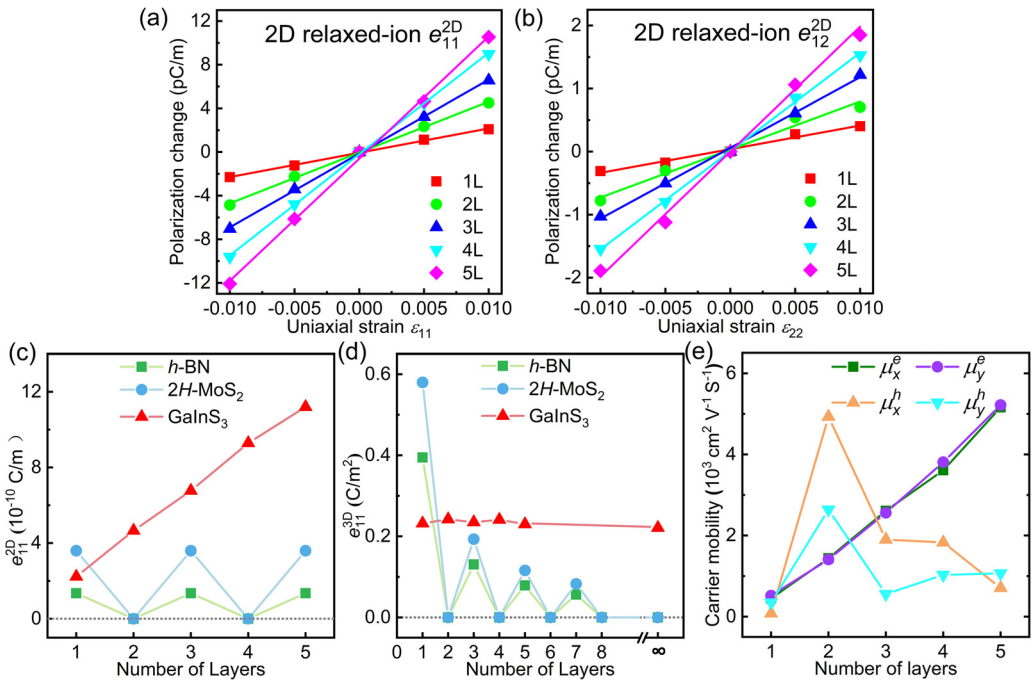

FIG. 3. 2D polarization changes along the x-direction with respect to applied uniaxial strains along (a) x- and (b) y-directions for $GaInS_3$ nanosheets. The 2D piezoelectric coefficients e_{11}^{2D} and e_{12}^{2D} can be obtained from the slopes of the lines. (c) 2D and (d) 3D piezoelectric coefficients e_{11}^{2D} and e_{11}^{3D} of $GaInS_3$, h-BN, and 2H-MoS_2 as a function of layer number N. (e) Layer-dependent carrier mobilities of 2D $GaInS_3$ nanosheets.

non-piezoelectric, while those with odd layers are noncentrosymmetric and possess non-zero piezoelectric coefficients.[3] Such odd-even effect also results in the rapid decrease in e_{11}^{3D} of h-BN and 2H-MoS_2 nanosheets with increasing N, which could finally vanish in the bulk [see Fig. 3(d)]. The results are consistent with those predicted theoretically and confirmed experimentally in MoS_2 systems, which have been found to largely restrict their applications in integrated piezoelectric devices.[1,3]

Due to the directly stacking structure of the unit cell along the x-direction accompanying with the uniform polarization [see Fig. 4(a)], monolayer and multilayer $GaInS_3$ could maintain the C_{2v} symmetry and exhibit robust in-plane piezoelectricity without the odd-even effect, which is consistent with those observed in α-In_2Se_3 nanoflakes and in clear contrast to those of h-BN and 2H-MoS_2 nanosheets. As shown in Fig. 3(d), e_{11}^{3D} of $GaInS_3$ nanosheets does not vary significantly with N and that of the monolayer (around 0.23 C/m^2) is well maintained in the nanosheets with different N, generally larger than those of h-BN and 2H-MoS_2 with increasing N. Similar behaviors of layer-dependent e_{12}^{3D}(around 0.04 C/m^2) are found for $GaInS_3$, as listed in the supplementary material, Table S3. Moreover, take the case of $GaInS_3$ bilayer, we also consider other possible stacking types, including polar (AB and AA) and nonpolar structures (AB′ and AA′) [see Fig. 4(b)]. The total energy difference ΔE between a possible stacking type and the ground state structure shows that the polar AB stacking is the most stable structure, which is consistent with the intrinsic bulk stacking type.

Based on Eq. (3), d_{11} and d_{12} are calculated based on the elastic stiffness constants C_{ij}, which can be determined by the finite difference method. As expected, the elastic stiffness constants satisfy the Born stability criteria described by the relations $C_{11}C_{22} - C_{12}^2 > 0$ and C_{11}, C_{22}, $C_{66} > 0$,[39] demonstrating the good mechanical stability of 2D $GaInS_3$ (see the supplementary material, Table S3). Moreover, due to the retention of noncentrosymmetry, d_{11} of multilayer $GaInS_3$ is maintained at a relatively stable level of 2.08–2.26 pm/V, which is comparable to that of α-quartz.[40] For 2D materials, the few-layer nanosheets can be easily synthesized experimentally, and one can customize the thickness of nanosheets discretionarily according to the piezoelectric application requirements. Therefore, the robust and anomalous layer-dependent piezoelectricity in $GaInS_3$ nanosheets could be promising for applications in energy harvesting and piezotronics.

The carrier mobility is another important factor that determines the practical performance of electronic and piezoelectric devices. Herein, the carrier mobilities of 2D $GaInS_3$ nanosheets are calculated based on the deformation potential theory as proposed by Bardeen and Shockley[41] and the mobility formula including the anisotropy of elastic stiffness constants, deformation potential, and effective mass as generalize by Lang *et al.*[42] (see computational details in the supplementary material) As shown in Fig. 3(e), the electron mobility increases gradually with increasing N and reaches as high as 5160 (5220) cm^2 V^{-1} s^{-1} along the x-direction (y-direction) for five-layer $GaInS_3$. Moreover, the bilayer structure exhibits the highest hole mobility of 4930 (2640) cm^2 V^{-1} s^{-1} along the x-direction (y-direction). The high carrier mobilities of $GaInS_3$ nanosheets are comparable to those of few-layer black phosphorus. The outstanding and layer-dependent carrier mobility could improve the applicability of $GaInS_3$ nanosheets in piezoelectric devices.

31 December 2024 04:21:12

Published under an exclusive license by AIP Publishing

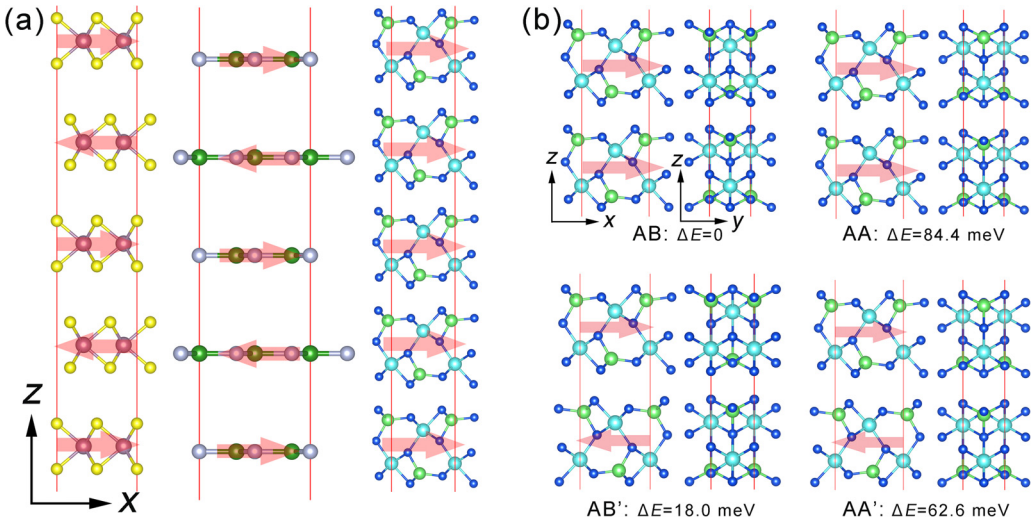

FIG. 4. (a) The stacking configurations of five-layer 2*H*-MoS_2, *h*-BN, and $GaInS_3$. (b) Side views of AB, AA, AB′, and AA′ stacking structures for bilayer $GaInS_3$. The red arrow represents the polarization direction of monolayer within one unit cell. AB stacking type, directly extracted from its bulk crystal, represents the ground state structure. ΔE is the total energy difference between a possible stacking type and the ground state structure.

In summary, we reported a class of 2D $GaInS_3$ semiconductors, which can be exfoliated from their bulk crystal. Theoretical calculations show that 2D $GaInS_3$ nanosheets have good thermal and structural stabilities and oxidation resistance, as well as tunable wide bandgap ranging from 2.66 eV (bulk) to 3.04 eV (monolayer). Due to the strain sensitivity of $GaInS_3$ nanosheets, the indirect-to-direct bandgap transition can be achieved under a small strain. Moreover, the particular stacking structure with C_{2v} symmetry endows 2D $GaInS_3$ nanosheets with promising piezoelectricity without the odd-even effect, which is much different with those of previously reported 2D piezoelectric materials. With the increasing number of layers, the piezoelectric stress and strain coefficients e_{11}^{3D} and d_{11} of 2D $GaInS_3$ nanosheets are sustained at a consistent level with those of monolayer (around 0.23 C/m^2 and 2.08 pm/V, respectively). The stability in piezoelectricity accompanying with high carrier mobility endows 2D $GaInS_3$ nanosheets with promising application prospects in nanosized sensors, piezotronics, and energy-harvesting devices. Those electronic and piezoelectric properties of $GaInS_3$ nanosheets as demonstrated in this work call for further practical applications and experimental verifications.

See the supplementary material for the computational details of carrier mobility, crystal configuration, and band structures of bulk $GaInS_3$ in Fig. S1, lattice parameters and bandgaps of $GaInS_3$ nanosheets in Table S1, structural changes of $GaInS_3$ monolayer with gaseous phase O_2 after AIMD simulation for 10 ps in Fig. S2, band structures of $GaInS_3$ monolayer under in-plane applied strains in Figs. S3–S5, band structures of $GaInS_3$ multilayers in Fig. S6, fitted parameters for layer-dependent bandgaps of $GaInS_3$ nanosheets in Table S2, piezoelectric coefficients of $GaInS_3$ nanosheets in Table S3, carrier mobilities of $GaInS_3$ nanosheets in Table S4, and evaluations of band edges of $GaInS_3$ nanosheets with respect to applied strains in Figs. S7–S11.

This work was supported by the National Natural Science Foundation of China (Nos. 21603056, 12047517, and 11904079), the Natural Science Foundation of Henan (No. 202300410069), the China Postdoctoral Science Foundation (Nos. 2019M652303, 2020TQ0089, and 2020M682274), and Foshan Xianhu Laboratory of the Advanced Energy Science and Technology Guangdong Laboratory. H.B.Y. acknowledges support from the Young Talents Program of Henan University.

DATA AVAILABILITY

The data that support the findings of this study are available from the corresponding author upon reasonable request.

REFERENCES

[1] J. Zhang and S. A. Meguid, Semicond. Sci. Technol. **32**(4), 043006 (2017).
[2] M. B. Ghasemian, T. Daeneke, Z. Shahrbabaki, J. Yang, and K. Kalantar-Zadeh, Nanoscale **12**(5), 2875–2901 (2020).
[3] W. Wu, L. Wang, Y. Li, F. Zhang, L. Lin, S. Niu, D. Chenet, X. Zhang, Y. Hao, T. F. Heinz, J. Hone, and Z. L. Wang, Nature **514**(7523), 470–474 (2014).
[4] H. Zhu, Y. Wang, J. Xiao, M. Liu, S. Xiong, Z. J. Wong, Z. Ye, Y. Ye, X. Yin, and X. Zhang, Nat. Nanotechnol. **10**(2), 151–155 (2015).
[5] M. M. Alyörük, Y. Aierken, D. Çakır, F. M. Peeters, and C. Sevik, J. Phys. Chem. C **119**(40), 23231–23237 (2015).
[6] M. N. Blonsky, H. L. Zhuang, A. K. Singh, and R. G. Hennig, ACS Nano **9**(10), 9885–9891 (2015).
[7] K.-A. N. Duerloo, M. T. Ong, and E. J. Reed, J. Phys. Chem. Lett. **3**(19), 2871–2876 (2012).
[8] R. Fei, W. Li, J. Li, and L. Yang, Appl. Phys. Lett. **107**(17), 173104 (2015).
[9] W. Li and J. Li, Nano Res. **8**(12), 3796–3802 (2015).
[10] R. Gao and Y. Gao, Phys. Status Solidi (RRL)–R **11**(3), 1600412 (2017).
[11] H. Yin, J. Gao, G.-P. Zheng, Y. Wang, and Y. Ma, J. Phys. Chem. C **121**(45), 25576–25584 (2017).
[12] K. H. Michel and B. Verberck, Phys. Rev. B **83**, 115328 (2011).
[13] F. Xue, J. Zhang, W. Hu, W.-T. Hsu, A. Han, S.-F. Leung, J.-K. Huang, Y. Wan, S. Liu, J. Zhang, J.-H. He, W.-H. Chang, Z. L. Wang, X. Zhang, and L.-J. Li, ACS Nano **12**(5), 4976–4983 (2018).
[14] G. G. Guseinov, I. R. Amiraslanov, and A. S. Kuliev, Kristallografiya **32**(1), 140–141 (1987).
[15] G. Kresse and J. Furthmüller, Phys. Rev. B **54**(16), 11169–11186 (1996).

31 December 2024 04:21:12

Published under an exclusive license by AIP Publishing

[16]G. Kresse and J. Furthmüller, Comput. Mater. Sci. **6**(1), 15–50 (1996).
[17]G. Kresse and D. Joubert, Phys. Rev. B **59**(3), 1758–1775 (1999).
[18]J. P. Perdew, K. Burke, and M. Ernzerhof, Phys. Rev. Lett. **77**(18), 3865–3868 (1996).
[19]P. E. Blöchl, Phys. Rev. B **50**(24), 17953–17979 (1994).
[20]H. J. Monkhorst and J. D. Pack, Phys. Rev. B **13**(12), 5188–5192 (1976).
[21]J. Heyd, G. E. Scuseria, and M. Ernzerhof, J. Chem. Phys. **118**(18), 8207–8215 (2003).
[22]S. Grimme, S. Ehrlich, and L. Goerigk, J. Comput. Chem. **32**(7), 1456–1465 (2011).
[23]L. Chaput, A. Togo, I. Tanaka, and G. Hug, Phys. Rev. B **84**(9), 094302 (2011).
[24]G. J. Martyna, M. L. Klein, and M. Tuckerman, J. Chem. Phys. **97**(4), 2635–2643 (1992).
[25]S. Jiang, J. Li, W. Chen, H. Yin, G.-P. Zheng, and Y. Wang, Nanoscale **12**(10), 5888–5897 (2020).
[26]W. Zhou, S. Guo, S. Zhang, Z. Zhu, X. Song, T. Niu, K. Zhang, X. Liu, Y. Zou, and H. Zeng, Nanoscale **10**(7), 3350–3355 (2018).
[27]U. M. Özgür, D. Hofstetter, and H. Morkoç, Proc. IEEE **98**, 1255–1268 (2010).
[28]Z. Wu, W. Jie, Z. Yang, and J. Hao, Mater. Today Nano **12**, 100092 (2020).
[29]C. Gong, J. Chu, C. Yin, C. Yan, X. Hu, S. Qian, Y. Hu, K. Hu, J. Huang, H. Wang, Y. Wang, P. Wangyang, T. Lei, L. Dai, C. Wu, B. Chen, C. Li, M. Liao, T. Zhai, and J. Xiong, Adv. Mater. **31**(36), 1903580 (2019).
[30]S. Zhang, Z. Yan, Y. Li, Z. Chen, and H. Zeng, Angew. Chem. Int. Ed. **54**(10), 3112–3115 (2015).
[31]B. Wang, X. Zhang, Y. Zhang, S. Yuan, Y. Guo, S. Dong, and J. Wang, Mater. Horiz. **7**(6), 1623–1630 (2020).
[32]H. Yin, C. Liu, G.-P. Zheng, Y. Wang, and F. Ren, Appl. Phys. Lett. **114**(19), 192903 (2019).
[33]C. Liu, B. Wang, G. Jia, P. Liu, H. Yin, S. Guan, and Z. Cheng, Appl. Phys. Lett. **118**(7), 072902 (2021).
[34]V. Tran, R. Soklaski, Y. Liang, and L. Yang, Phys. Rev. B **89**(23), 235319 (2014).
[35]B. Wang, X. Niu, Y. Ouyang, Q. Zhou, and J. Wang, J. Phys. Chem. Lett. **9**(3), 487–490 (2018).
[36]J. F. Nye, *Physical Properties of Crystals: Their Representation by Tensors and Matrices* (Oxford University Press, New York, 1985).
[37]R. D. King-Smith and D. Vanderbilt, Phys. Rev. B **47**(3), 1651–1654 (1993).
[38]D. Vanderbilt, J. Phys. Chem. Solids **61**(2), 147–151 (2000).
[39]F. Mouhat and F.-X. Coudert, Phys. Rev. B **90**(22), 224104 (2014).
[40]R. Bechmann, Phys. Rev. **110**(5), 1060–1061 (1958).
[41]J. Bardeen and W. Shockley, Phys. Rev. **80**(1), 72–80 (1950).
[42]H. Lang, S. Zhang, and Z. Liu, Phys. Rev. B **94**(23), 235306 (2016).

31 December 2024 04:21:12

Published under an exclusive license by AIP Publishing